The Nuclear Field Theory

Daniel R. BES

Physics Department, Comision Nacional de Energia Atomica
Buenos Aires

(Received August 9, 1982)

The nuclear field theory (NFT) is presented here with particular emphasis on its foundations. The following points are discussed: i) the equivalence between pure fermion and NFT operators (including the Hamiltonian), ii) the results from an exactly soluble example, iii) the appropriate expansion parameter and the convergence of the corresponding perturbation series and iv) the extension to deformed systems. This is accomplished through the derivation of both the deformed Hamiltonian (superfluid case) and of the perturbational treatment appropriate for deformed basis.

§ 1. Elementary modes of excitation

They represent a generalization of the concept of the normal modes of vibrations in a classical system. Thus, they provide a basis for expressing the complicated excitations that can be produced in the neighbourhood of a given equilibrium configuration. In addition to this practical purpose of economy in expressing the complicate spectra in terms of relatively few building blocks, the study of the elementary modes is important because the deeper properties of the system are reflected in the nature of these building blocks.

The concept of elementary modes was introduced in Fermi systems by Landau.[1] Their importance in nuclear physics has been specially stressed by the Copenhagen School.[2]

The mathematics of the elementary modes is simple. Let us assume that it is possible to recast the many-body Hamiltonian (including a two-body term) as a summation of Hamiltonians H_σ' corresponding to separate degrees of freedom.

$$H \to \sum_\sigma H_\sigma' \,. \tag{1}$$

The energy of the states (for at any rate, of the most important states in order to determine the physical response of the system to external probes) has the form

$$E = \sum_\sigma n_\sigma \varepsilon_\sigma \,, \tag{2}$$

where ε_σ are the eigenvalues of H_σ'. The eigenstates of the total system are

$$|n\rangle = \prod_\sigma (n_\sigma!)^{-1/2} (\Gamma_\sigma^\dagger)^{n_\sigma} |0\rangle . \tag{3}$$

Here $n_\sigma = 0$ or 1 in the case of fermions and $n_\sigma = 0, 1, 2, \cdots$ in the case of bosons. The operator $\Gamma_\sigma^\dagger$ creates an excitation with quantum number σ, when acting on the state $|0\rangle$ (the vacuum of all the excitations σ). Additivity features similar to (2) hold also for transition matrix elements.

With the help of experimental probes which couple weakly to the nucleus (i.e., in such a way that the system can be expressed in terms of the properties of the excitation in the absence of probes) it has been possible to identify the elementary modes which are listed in Table I. As an example, Fig. 1 represents the known states belonging to the family of neutron monopole pairing modes in the Pb region. Similarly, Table II contains the information

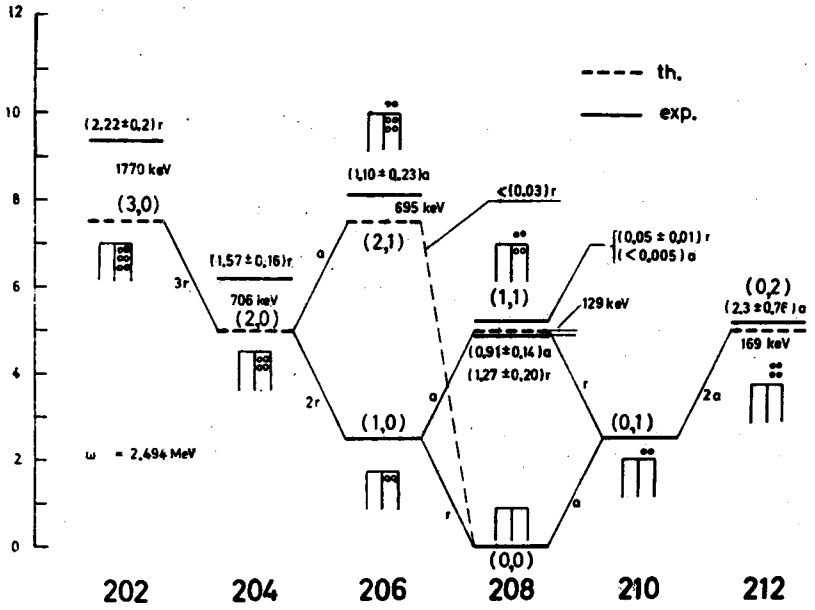

Fig. 1. The many-phonon neutron pairing spectrum around ^{208}Pb (Ref. 17)). The energies predicted by the pairing vibration model are displayed as dotted horizontal lines while the experimental values are drawn as continuous lines. The harmonic quantum numbers (n_r, n_a) are indicated for each level. A schematic representation of the many-particle many-hole structure of the state is also given. The transitions predicted by the model are indicated in units of r and a. The corresponding experimental numbers are also given together with their errors above each level. The dotted line between the states (0, 0) and (2, 1) indicates that the ^{208}Pb(p, t) ^{206}Pb reaction to the three-phonon states in ^{206}Pb was carried out and an upper limit of $0.03r$ for corresponding cross section was determined.

concerning the single-neutron degree of freedom in the same region. From Fig. 1 and Table II we conclude that (at least) the collective pairing modes and the fermion modes coexist in the Pb region. Our aim is to describe the collective and single-particle degrees of freedom on an equal footing. Subsequently, the residual couplings should be treated through a perturbative expansion (NFT).

Table I. Elementary modes of excitation in nuclei (Ref. 3)). The rotations have been excluded since they do not satisfy the addititivity criteria.

mode	formalism	specific excitation mechanism experiment
single-particle motion	$a^\dagger(\nu)$, $a(\nu)$	single-particle addition or removal
density oscillations	$(a^\dagger a)$	
shape	$a^\dagger(j)a(j')$	
isospin	$[(a^\dagger a)_n-(a^\dagger a)_p]$	inelastic scattering
others	.....	
pair vibrations	$a^\dagger(j)a^\dagger(j')$	two-particle transfer
nucleonic excitation		
"(33) resonance"	$a_\pi^\dagger a_\pi$	pion scattering
hyper nuclei	$(c_\pi^\dagger c_K)$	$(K\pi)$ exchange

Table II. Single-neutron states in the region around Pb^{208}. The excitation energies E in the residual nucleus, the transferred angular momentum Δl and the spectroscopic factors S are given for Pb^{208} (d, p) Pb^{209} reactions and $E<3$ MeV (Ref. 46)). The validity of the independent particle model becomes established by the fact that there are transitions with spectroscopic factors S close to the sum rule value 1, while all others S almost vanish. Moreover, there is a biunivocal correspondence between the states with $S\simeq 1$ and those predicted by realistic central potentials (last column).

E (MeV)	l	S	Shell model configuration
0	4	0.83	$2g_{9/2}$
0.779	6	0.86	$1i_{11/2}$
1.424	7	0.58	$1j_{15/2}$
1.565	2	0.98	$3d_{5/2}$
2.033	0	0.98	$4s_{1/2}$
2.152	1	0.007	
2.319	1	0.007	
2.464	3	0.001	
2.493	4	1.05	$2g_{7/2}$
2.537	2	1.09	$3d_{3/2}$
2.592	5	0.018	
2.738	3	0.003	
2.866	3	0.001	

"The central theme is the dialectic between classical macroscopic pictures and the microscopic quantal structures that emerge as soon as one expresses those pictures in terms of the motions of neutrons and protons that move in quantized orbits exhibiting shell structure".[3]

§ 2. Feynman's diagrams and the graphical perturbative derivation of the NFT

In quantum mechanics, we deal with the amplitudes to get from the initial state at time t to the final state at time t'. A great advantage of these amplitudes (Green's functions) is that a useful and elegant graphical perturbation theory is obtained from them. Each diagram is as precise as an equation and, in addition, it represents the detailed evolution of the system.*) In the following, we review some known results obtained through this technique. For more details see, for instance, Refs. 4) and 5).

The above-mentioned amplitudes, for the one-particle case, are

$$G(j', j; t'-t) = \langle 0|T\{a_{j'}(t')\, a_j^\dagger(t)\}|0\rangle, \tag{1}$$

where T orders the operators $a_{j'}(t')$, $a_j^\dagger(t)$ in a time sequence that increases from right to left. Introducing a complete set of states $|a\rangle$, $|r\rangle$ of the system with one particle more and less than the ground state, respectively, Eq. (1) reads

$$\begin{aligned} G(j', j;\ t'-t) = &\sum_a \langle 0|a_{j'}|a\rangle\langle a|a_j^\dagger|0\rangle e^{-i(E_a-E_0)(t'-t)}\theta(t'-t) \\ &-\sum_r \langle 0|a_j^\dagger|r\rangle\langle r|a_{j'}|0\rangle e^{-i(E_r-E_0)(t'-t)}\theta(t-t'). \end{aligned} \tag{2}$$

For a system of independent fermions, $|0\rangle$ represents a Slater determinant. Therefore, the one-body Green's function describes the propagation of a particle above the Fermi level if $t'>t$ and of a hole below the Fermi level if $t'<t$. Assuming a representation which diagonalizes the Hamiltonian,

$$\begin{aligned} &G(j', j; t'-t) = G_0(j, t'-t)\,\delta_{jj'}, \\ &G_0(j, t) = (1-n_j)\,\theta(t)\, e^{-i\epsilon_j t} - n_j\theta(-t)\, e^{i\epsilon_j t}. \end{aligned} \tag{3}$$

Using the same formalism, we describe the propagation of a particle-hole pair

$$\begin{aligned} G_{\rm ph}(jj', j''j''';\ t'-t) &= \langle 0|T\{a_{j'}^\dagger(t')\, a_j(t')\, a_{j''}^\dagger(t)\, a_{j'''}(t)\}|0\rangle \\ &= \sum_n \langle 0|a_{j'}^\dagger a_j|n\rangle\langle n|a_{j''}^\dagger a_{j'''}|0\rangle\theta(t'-t)\, e^{-iW_n(t'-t)} \end{aligned}$$

*) Moreover, it can even be beautiful.

$$+\sum_n \langle 0|a^\dagger_{j'}a_{j''}|n\rangle\langle n|a^\dagger_{j''}a_j|0\rangle\theta(t-t')\,e^{iW_n(t'-t)}, \tag{4}$$

which in the case of a free propagator simplifies to

$$\begin{aligned} G^{(0)}_{\rm ph}(jj', j''j''';\, t'-t) &= \delta_{jj''}\delta_{j'j'''}[(1-n_j)\,n_{j'}\theta(t'-t)\,e^{-i(\epsilon_j-\epsilon_{j'})(t'-t)} \\ &\quad + n_j(1-n_{j'})\,\theta(t-t')\,e^{i(\epsilon_{j'}-\epsilon_j)(t'-t)}] \\ &= -\delta_{jj''}\delta_{j'j'''}G_0(j,\, t'-t)\,G_0(j',\, t-t'). \end{aligned} \tag{5}$$

A non-interacting particle-hole state behaves like a free phonon, since one may distinguish between them only through their correlations and interactions with other particles or holes (i.e., in cases in which they are not free). Therefore, we may infer the expression for the propagator of a free-boson from (5):

$$G_B(n,\, t'-t) = e^{-i\omega_n(t'-t)}\theta(t'-t) + e^{i\omega_n(t'-t)}\theta(t-t'). \tag{6}$$

If we have a more complicated problem (such as a problem of interacting particles) the propagator may be written as a sum over all the alternative ways in which the particles can go from the initial to the final states. For instance, in the case of a particle-hole pair:

i) The particle-hole pair may not be scattered at all (Eq. (5)).

ii) The particle-hole pair may be scattered once

$$\begin{aligned} G^{(1)}_{\rm ph}(jj', j''j''';\, t'-t) &= -i\langle jj'''|V|j''j'\rangle \\ &\quad \times \int d\tau G_0(j'',\, \tau-t)\,G_0(j''',\, t-\tau)\,G_0(j,\, t'-\tau)\,G_0(j',\, \tau-t'). \end{aligned} \tag{7}$$

iii) The particle-hole pair may be scattered twice

$$\begin{aligned} G^{(2)}_{\rm ph}(jj', j''j''';\, t'-t) &= -\sum_{j_a, j_b}\langle jj_b|V|j_aj'\rangle\langle j_aj'''|V|j''j_b\rangle \\ &\quad \times \int d\tau' d\tau G_0(j'',\, \tau-t)\,G_0(j''',\, t-\tau)\,G_0(j_a,\, \tau'-\tau) \\ &\quad \times G_0(j_b,\, \tau-\tau')\,G_0(j,\, t'-\tau')\,G_0(j',\, \tau'-t'). \end{aligned} \tag{8}$$

iv) etc.

In the propagation of a particle-hole pair, let us consider only those diagrams in which a particle-hole pair is created and annihilated without interacting with other lines of the diagram. Thus, diagrams 2(a), (b) and (c) belong to this subset, while 2 (d) does not. This whole subset of diagrams is taken into account in the Bethe-Salpeter equation:

$$\begin{aligned} G_{\rm ph}(jj', j''j''';\, t'-t) &= G^{(0)}_{\rm ph}(jj', j''j''';\, t'-t) \\ &\quad -i\sum_{j_a, j_b}\langle j_aj'''|V|j''j_b\rangle \end{aligned}$$

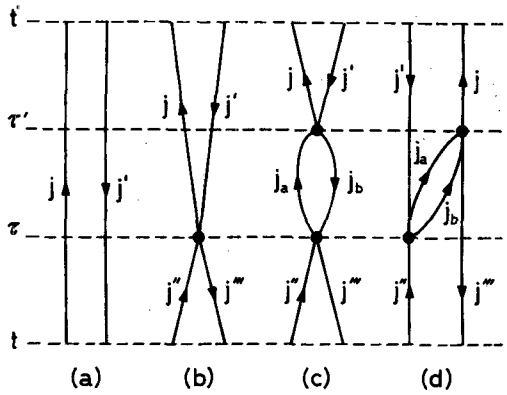

Fig. 2. Diagrams representing the propagation of a particle-hole pair in lowest orders of perturbation theory.

$$\times \int d\tau G^{(0)}_{\rm ph}(j_a j_b, j'' j'''; \tau - t) G_{\rm ph}(jj', j_a j_b; t' - \tau), \tag{9}$$

as can be seen by iteration. Using (4) and (5) and Fourier transforming, the following equations must be satisfied by the amplitudes $\langle n|a_j^\dagger a_{j'}|0\rangle$ at the poles corresponding to the energies W_n:

$$\langle n|a_j^\dagger a_{j'}|0\rangle = \frac{[(1-n_j)n_{j'} - n_j(1-n_{j'})]}{W_n - \varepsilon_j + \varepsilon_{j'}} \sum_{j''j'''} \langle j''j'''|V|jj'\rangle \langle n|a^\dagger_{j''}a_{j'''}|0\rangle. \tag{10}$$

This can be cast into the familiar matrix equation

$$\begin{bmatrix} A & B \\ -B & -A \end{bmatrix} \begin{bmatrix} X \\ Y \end{bmatrix} = W \begin{bmatrix} X \\ Y \end{bmatrix}, \tag{11}$$

where

$$(\mathrm{A}) = (e_k - e_i)\delta((ki), (k'i')) + \langle k'i|V|ki'\rangle; \quad (\mathrm{B}) = \langle i'i|V|kk'\rangle. \tag{12}$$

The amplitudes are

$$X(n, ki) = \langle n|a_k^\dagger a_i|0\rangle; \quad Y(n, ki) = \langle n|a_i^\dagger a_k|0\rangle. \tag{13}$$

Here $e_k > e_F$ and $e_i \leq e_F$ = Fermi energy. An application of (11) is given in Fig. 3.

Thus we have learned which diagrams have been taken into account in the replacement of "dressed" particle-hole states by phonons. Indeed, in this replacement an infinite subset of diagrams have been summed up. But this also implies that many others have been neglected. If more than a particle and a hole line would be present in the initial state, and each pair of particle-hole lines gives rise to a boson, we are neglecting interactions between fermion

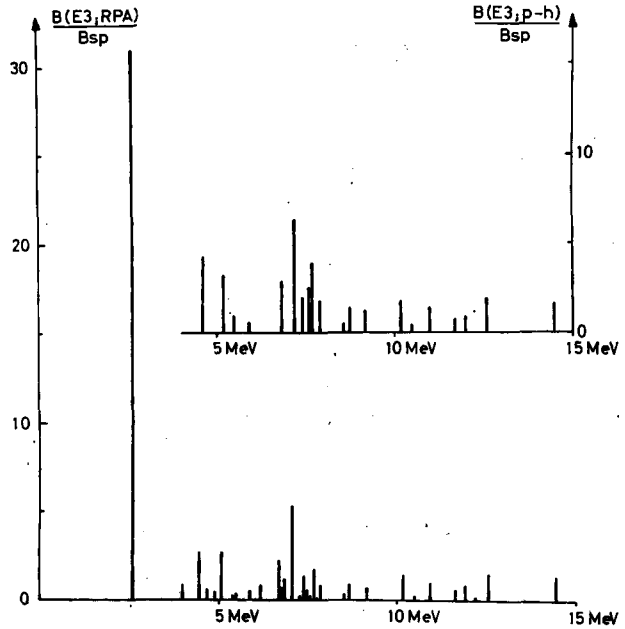

Fig. 3. The response function corresponding to the octupole modes in Pb^{208}. The calculation has been made using the experimentally known single-proton and single-neutron levels in Bi^{209}, Pb^{209}, Tl^{207} and Pb^{207}. In the upper part, the $B(E3)$ values for exciting particle-hole states are given in single-particle units. Only transitions with an intensity larger than 0.2 are indicated. An effective charge of $1.13e$ for protons and $0.13e$ for neutrons has been used in order to take into account polarization effects associated with the $\Delta N=3$ modes. The lower part of the figure represents the response function for the RPA normal modes. The same renormalized charges have been used. The coupling strength of the residual octupole interaction has been fixed so that the lowest 3^- state lies at 2.62 MeV. The $B(E3)$ value corresponding to the collective state is $31B_{sp}$ in agreement with the experimental value $39B_{sp}$. For both the upper and lower figure, the energy weighted sum rule is $\sum_n W_n B(E3, n) = 325 B_{sp}$ MeV.

lines belonging to different pairs. In particular, we are violating the Pauli principle, which is taken into account provided that for a given diagram, those obtained by interchanging the end points of the fermion line are also considered.

Unlike the propagation considered in (4), where $t_1 = t_2$ and $t_3 = t_4$, we consider now the propagation of two fermion lines in a given Feynman diagram, such that the two lines appear and disappear at different vertices. The propagation of the two lines yields the Green's function

$$G(j_1 t_1, j_2 t_2, j_3 t_3, j_4 t_4) = \langle 0 | T\{a^\dagger_{j_1}(t_1)\, a_{j_2}(t_2)\, a^\dagger_{j_3}(t_3)\, a_{j_4}(t_4)\} | 0 \rangle . \qquad (14)$$

If $t_1 > t_2 > t_3 > t_4$ (for instance), the zero and first order contributions to the propagator are

$$G^{(0)} = -G_0(j_1; t_4 - t_1) G_0(j_2; t_2 - t_3) \delta_{j_1 j_4} \delta_{j_2 j_3},$$

$$G^{(1)} = -i \langle j_2 j_4 | V | j_1 j_3 \rangle \int d\tau G_0(j_2, t_2 - \tau) G_0(j_1, \tau - t_1) G_0(j_3, \tau - t_3) G_0(j_4, t_4 - \tau). \tag{15}$$

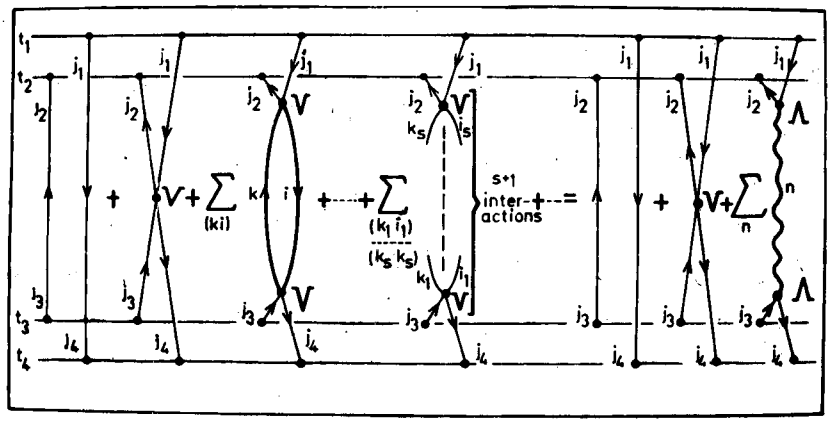

Fig. 4. Correspondence between the Feynman diagrammatic expansion of the propagator in the pure fermion treatment (left) with the Feynman diagrams associated with the same propagator in the NFT (right) (Ref. 9)).

Among the second order contributions, we consider the one in which there is a particle-hole pair propagating between τ and τ' (Fig. 4). There are also higher-order contributions in which this intermediate particle-hole pair is scattered an arbitrary number of times by the interaction. The propagation between τ and τ' is given by the Green's function (4)

$$\sum_{\nu \geq 2} G^{(\nu)} = -\sum_{jj'j''j'''} \langle j_2 j | V | j_2 j' \rangle \langle j'' j_4 | V | j''' j_3 \rangle \int d\tau d\tau' G_0(j_2, t_2 - \tau') \times G_0(j_1, \tau' - t_1) G_{\mathrm{ph}}(j_2 j_1, j_3 j_4; \tau' - \tau) G_0(j_3, \tau - t_3) G_0(j_4, t_4 - \tau). \tag{16}$$

By replacing (4) and (13) into (16), we obtain

$$\sum_{\nu \geq 2} G^{(\nu)} = -\int d\tau d\tau' G_0(j_2, t_2 - \tau') G_0(j_1, \tau' - t_1) G_0(j_3, \tau - t_3) G_0(j_4, t_4 - \tau) \times \sum_n \{ A(j_2 j_1; n) A(j_3 j_4; n) e^{-iW_n(\tau' - \tau)} \theta(\tau' - \tau) + A(j_1 j_2; n) A(j_4 j_3; n) e^{iW_n(\tau' - \tau)} \theta(\tau - \tau') \}, \tag{17}$$

where

$$A(j_a j_b; n) = \sum_{jj'} \langle j_a j | V | j_b j' \rangle \langle 0 | a_j^\dagger a_{j'} | n \rangle. \tag{18}$$

In (18) the restriction is made that there should be one particle and

one hole present in each pair (jj').

The partial summation in (17) corresponds to replace the original fermion Hamiltonian by another Hamiltonian in which extra collective degrees of freedom are included. The factor within curly brackets in (17) has the same time-reversal properties as the propagator of a free phonon with energy W_n (Eq. (6)). The summation over n accounts for all the diagrams in which a particle and a hole line mutually interact ν number of times ($\nu \geq 2$). The propagation of each mode n is represented by a wavy line. The question whether a wavy line corresponds to the propagation of a true phonon or of a particle-hole pair is irrelevant, since there is no way to distinguish between them: to investigate this difference, another fermion line has to interact with either the particle or the hole line. However, we have assumed that both the particle-hole pair and the phonon propagate without interacting with any other line of the diagram between their creation and annihilation.

The crossing of a wavy line with another line of the diagram (either a fermion line or another wavy line) corresponds to an even number of crossings between fermion lines. Therefore, it does not introduce any extra minus sign, as the crossing between two fermion lines does. This is a further evidence of the identical behavior of the propagators of a boson and a particle-hole pair.

The factors $\Lambda(j_a j_b; n)$ represent the amplitude for the creation and annihilation of a phonon n and a single fermion transition from the state j_b to the state j_a (Fig. 4). They should thus be considered as the strength of the particle-phonon interaction. However, these vertices do not exhaust the effects of the two-body residual interaction. In fact, the four-point vertices still give a contribution through $G^{(1)}$. We thus justify the replacement of the fermion Hamiltonian by the nuclear field Hamiltonian introduced in Ref. 6), namely,

$$
\begin{aligned}
H_f &= H_{sp} + H_{tb} + H_b + H_{pv}\,, \\
H_{sp} &= \sum_j \varepsilon_j a_j^\dagger a_j\,; \quad H_b = \sum_n W_n \Gamma_n^\dagger \Gamma_n\,, \\
H_{tb} &= \frac{1}{4} \sum_j \langle j_1 j_2 | V | j_3 j_4 \rangle a_{j_1}^\dagger a_{j_2}^\dagger a_{j_3} a_{j_4}\,, \\
H_{pv} &= \sum_{nj} [\Lambda(j_1 j_2; n) \Gamma_n^\dagger a_{j_2}^\dagger a_{j_1} + \Lambda(j_1 j_2; n) \Gamma_n a_{j_1}^\dagger a_{j_2}]. \qquad (19)
\end{aligned}
$$

The exact results*) of the fermion Hamiltonian are reproduced by (19), provided the following rules are followed:

1) The couplings are allowed to act in all orders to generate the different diagrams of perturbation theory. All vertices of the fermion two-body inter-

*) These results appear as a consequence of the fact that both the original fermion Hamiltonian $H = H_{sp} + H_{tb}$ and the NFT Hamiltonian H_f (plus rules 1)~4)) yield the same Green's functions.

action and of the particle-vibration interaction have to be included, and all time permutations of these vertices in a given diagram have to be taken into account.

2) The internal lines of diagrams are restricted by the exclusion of diagrams in which a particle-hole pair is created and subsequently annihilated without having participated in the meantime in the interaction with another lines (bubles). This rule is due to the fact that all the diagrams with this feature have been replaced by diagrams in which phonons propagate. Because of this rule, only a diagrammatic treatment appears to be feasible.

3) The energies and coupling constants of the phonon field are determined by the energies W_n and amplitudes $X(n, jj')$, $Y(n, jj')$ of the perturbed propagator of a particle-hole pair. The simplest method to obtain these quantities is through the RPA (Eqs. (11)$\sim$(13)). However, we may also use more complicated irreducible vertex parts and, consequently, generalize the concept of buble.[7]

4) The collective and fermion degrees of freedom are mutually orthogonal

$$[\Gamma_n^\dagger, a_j^\dagger] = [\Gamma_n, a_j^\dagger] = 0 , \tag{20}$$

and they interact only through (19) plus the restriction 2). In particular, $|0\rangle$ is the vacuum state both for fermion and bosons, namely,

$$\Gamma_n|0\rangle = a_k|0\rangle = a_i^\dagger|0\rangle = 0 . \tag{21}$$

The equivalence between the field Hamiltonian (19) and the original fermion Hamiltonian has thus been established for the internal parts of a diagram. The question whether the external lines should be either phonons n or the original particle-hole lines (k, l) was empirically answered in Ref. 6) in favour of the phonons. We may divide the diagrams in two groups: in initial or final states, proper diagrams involve collective modes n and particle modes j, but not particle-hole configuration that can be replaced by a combination of collective modes. For instance, the initial state of the type $\Gamma_n^\dagger a_k^\dagger|0\rangle$ corresponds to a proper diagram, but $a_k^\dagger a_{k'}^\dagger a_{i'}|0\rangle$ to an improper one. The proof that improper states are not normalizable and thus cannot be used as initial or final states is given in Ref. 7).

The interaction of the system with an external field is proportional to the one-body operator

$$Q = \sum_{jj'} \langle j|Q|j'\rangle a_j^\dagger a_{j'} . \tag{22}$$

Any fermion diagram that describes the effect of (22) contains two fermion lines (jj') having a common vertex $\langle j|Q|j'\rangle$ at an instant t_0. These two lines are included within a section of the total diagram, such that this section joins the remaining part of the diagram through the two "external" fermion lines

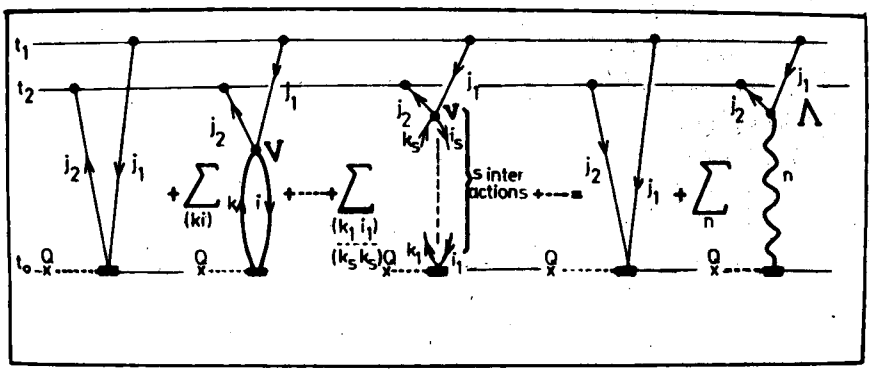

Fig. 5. Correspondence between the Feynman diagrammatic expansion describing the effect of an external single particle operator Q in the pure fermion treatment (left) with the Feynman diagrams associated with the same process in the NFT (right) (Ref. 9)).

$(j_1 j_2)$ at the instants t_1 and t_2 $(t_1 \neq t_2)$, respectively (see Fig. 5). The contribution of this section to the time evolution of the system is

$$G_Q = \sum_{jj'} \langle j|Q|j'\rangle G(j_1 t_1, j_2 t_2, jt_0, j' t_0). \tag{23}$$

In addition to the case of free propagation within the section, let us consider those cases in which the two lines $(j_1 j_2)$ have a common interaction vertex at the time τ, which is also common to the "internal" particle-hole pair, $(j_3 j_4)$. We also assume that (jj') corresponds to a particle-hole pair. Applying the same arguments as before, Eq. (23) can be written in terms of the usual particle-hole Green's function G_{ph} which depends on a single time difference $\tau - t_0$:

$$\begin{aligned} G_Q = & -\langle j_2|Q|j_1\rangle G_0(j_2, t_2 - t_0) G_0(j_1, t_0 - t_1) \\ & - (-i)\langle j|Q|j'\rangle\langle j_2 j_4|V|j_1 j_3\rangle \\ & \times \int d\tau G_0(j_2, t_2 - \tau) G_0(j_1, \tau - t_1) G_{\mathrm{ph}}(j_3 j_4 j j'; \tau - t_0). \end{aligned} \tag{24}$$

In order to obtain the field representation of the operator Q, we use also in (24) Eqs. (4) and (13):

$$\begin{aligned} G_Q = & -\langle j_2|Q|j_1\rangle G_0(j_2, t_2 - t_0) G_0(j_1, t_0 - t_1) \\ & - (-i) \int d\tau G_0(j_2, t_2 - \tau) G_0(j_1, \tau - t_1) \\ & \times \sum_n [A(j_2 j_1, n)\langle n|Q|0\rangle e^{-iW_n(\tau - t_0)}\theta(\tau - t_0) \\ & + A(j_1 j_2, n)\langle 0|Q|n\rangle e^{iW_n(\tau - t_0)}\theta(t_0 - \tau)], \end{aligned} \tag{25}$$

where

$$\langle n|Q|0\rangle=\sum_{ki}\left[\langle k|Q|i\rangle X(n,ki)+\langle i|Q|k\rangle Y(n,ki)\right]. \tag{26}$$

The first term in (25) represents the amplitude for the transition between the single-particle states $(j_1 j_2)$. The second term accounts for a whole set of diagrams in which an initial particle and an initial hole states successively interact.

The coefficients (26) represent the amplitude with which the phonon is created or annihilated by the operator Q.

Therefore, in the field formalism, the operator Q_f contains both a fermion term Q and boson term Q_b,

$$\begin{aligned} &Q_f=Q+Q_b\,,\\ &Q=\sum_{jj'}\langle j|Q|j'\rangle a_j^{\dagger}a_{j'}\,,\\ &Q_b=\sum_{n}\langle n|Q|0\rangle\Gamma_n^{\dagger}+\langle 0|Q|n\rangle\Gamma_n\,. \end{aligned} \tag{27}$$

We have thus proven the complete equivalence between the fermion Hamiltonian and single-particle operators with the NFT operators (19) and (27). This equivalence can be derived for any many-body operator.[8]

It is clear, however, that the NFT basis is overcomplete. The non-hermiticity of the NFT Hamiltonian (due to the restriction 2)) eliminates the spurious states from the final results, as seen in § 3.

The same arguments can be carried over for the situation in which the successive interactions take place between two-particle or two-hole lines (pairing phonons). The set of diagrams in which the two lines interact ν number of times $(\nu\geq 2)$ is replaced by a single diagram in which an addition-type or removal-type pairing boson is present.

The present derivation of the NFT can be found in Ref. 9). See also Refs. 10), 11) and 12). The NFT has also been obtained within the TDA and the Wigner-Brillouin perturbation expansion in Ref. 13). In Ref. 13)

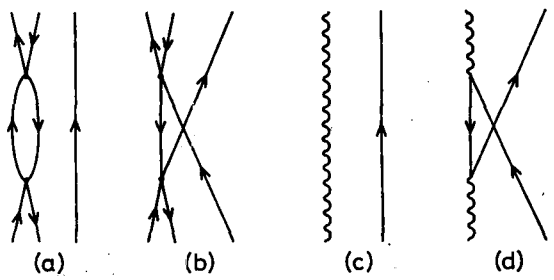

Fig. 6. Pure fermion (a), (b) and corresponding NFT diagrams (c), (d) including corrections due to the Pauli principle.

one of the few existing comparisons between the NFT and other boson expansions is made (in this case, with the Dyson boson expansion; see also Ref. 14)).

In pure fermion Feynman diagrams, intermediate states are not antisymmetrized. The Pauli principle is taken care by the exchange diagrams as in Figs. 6(a) and (b). These two diagrams are part of a series which is summed up within NFT, yielding the free particle-phonon propagator (Fig. 6(c)) and diagram 6(d), respectively.

The introduction of diagram 6(d) by Mottelson[15] was a crucial step in developing the NFT. They should not be interpreted as giving rise to a two-particle one-hole admixture in the predominantly particle-phonon state, but rather as an elimination of Pauli violating components in this state. These diagrams include vertices through which a phonon gives rise to a particle-hole state. This is consistent with rules 1) and 4), implying the orthogonality of phonon and particle-hole states within the NFT formalism, in spite of microscopic origin of the phonons.

§ 3. Application to an exactly soluble model

The model[16),17)] consists of Ω double degenerate $(m, \bar{m})$ single-particle states in which three particles are coupled through a pairing force

$$\begin{aligned} H &= H_{sp} + H_p \,, \\ H_{sp} &= \sum_m e_m a_m^\dagger a_m \,, \\ H_p &= -V \sum_m{}' \, a_m^\dagger a_{\bar{m}}^\dagger \sum_{m'}{}' \, a_{\bar{m}'} a_{m'} \,. \end{aligned} \tag{1}$$

There is no Hartree-Fock contributions from H_p to H_{sp}. Here $\sum_m' = \sum_{m>0}$.

The phonon energies ω_ν and the corresponding particle-vibration coupling constants Λ_ν are determined through the RPA (TDA) relations

$$V^{-1} = \sum_m{}' \, (2e_m - \omega_\nu)^{-1} \,, \tag{2}$$

$$\Lambda_\nu = \langle n_\nu = 1 | H_p | a_m^\dagger a_{m'}^\dagger \rangle = \delta_{m',\bar{m}} [\sum_{m''}{}' \, (2e_{m''} - \omega_\nu)^2]^{-1/2} \,. \tag{3}$$

The Ω different frequencies ω_ν are also the exact energies of the states with $M=0$ $(M = m + m')$ in the two-particle system. Consistently, there are no diagrammatic NFT corrections to the one boson states. Since the states $(m, \bar{m})$ are only allowed as intermediate states (proper diagrams) no over-counting of initial or final states is made in this case. However, for the three particle system, there are also Ω states $|n_\nu = 1; m\rangle$ which are allowed as proper initial or final states, but there are only $\Omega - 1$ physical states with $M = m$, in which the odd particle is in the state m. Therefore, a spurious state exists in the proper spectrum.

In the present section we isolate this spurious component, which a priori has a non-zero projection over all the states $|n_\nu=1, m\rangle$.

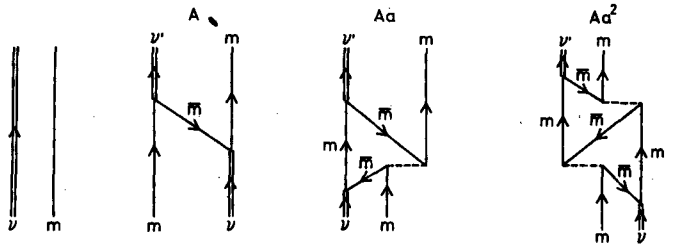

Fig. 7. Lowest order contributions to the energy matrix element between the basis states $|n_\nu=1, m\rangle$. The dotted line stands for the model bare interaction (Eq. (1)).

We divide the Hilbert space into particle-phonon states (model space) and three-particle states. The unperturbed energy of the states belonging to the model space is $\omega_\nu+e_m$. Use is made of the Bloch-Horowitz perturbative theory. The effective matrix elements $W_{\nu\nu'}(E)$ between these states are constructed as in Fig. 7, with

$$A=-\Lambda_\nu\Lambda_{\nu'}/(E-\varepsilon_m),$$
$$a=-V/(E-\varepsilon_m),$$
$$\varepsilon_m=3e_m. \tag{4}$$

The total value is

$$W_{\nu\nu'}(E)=\langle n_\nu=1, m|H|n_{\nu'}=1, m\rangle=A\sum_n a^n=\frac{A}{1-a}$$
$$=-\Lambda_\nu\Lambda_{\nu'}/(E-\varepsilon_m-V). \tag{5}$$

The secular equation

$$|E\delta_{\nu\nu'}-W_{\nu\nu'}(E)|=0 \tag{6}$$

is equivalent to the dispersion relation

$$F_m(E)\equiv\sum_\nu \Lambda_\nu^2/(\omega_\nu+e_m-E)=E-\varepsilon_m-V. \tag{7}$$

The relation (7) can be solved graphically as shown in Fig. 8. With some algebra we see that the energy $E_{qm}=\varepsilon_m$ is always a double root (the line $E=\varepsilon_m-V$ is tangent to $F_m(E)$ at $E=\varepsilon_m$). The remaining intersections of this line and the function $F_m(E)$ give rise to $\Omega-1$ additional roots E_q, which agree with the exact results.

The amplitude $\zeta_{q,\nu}$ of each state $|n_\nu=1, m\rangle$ in the eigenstates $|q\rangle$ are

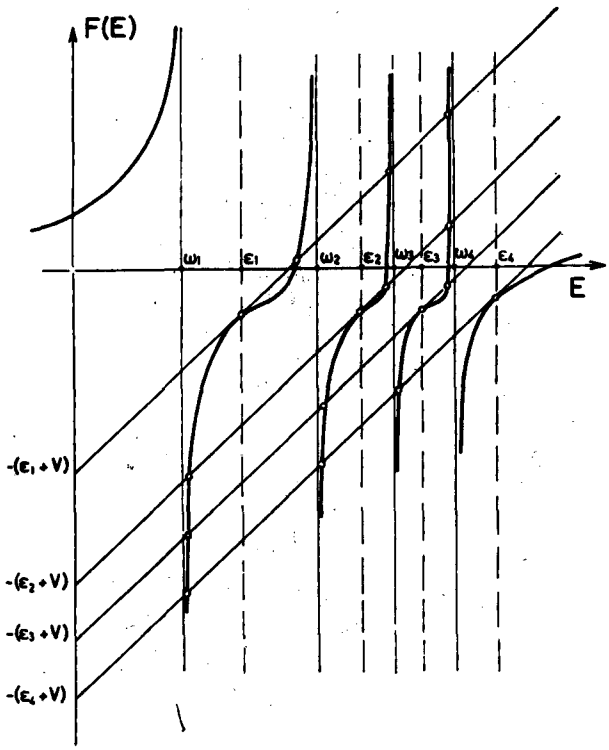

Fig. 8. Graphical solution of the dispersion relation (7) for the case $\Omega=4$ (Ref. 16)). The function $F_m(E)$ is displayed as a continuous thick line while the parallel lines $E-\varepsilon_m-V$ have been drawn as thin continuous lines intersecting the ordinate axis at (ε_m+V). The intersections between the two functions give the eigenvalues of the secular equation. For each value of ε_m there are $\Omega+1$ roots, the roots at $E=\varepsilon_m$ being double.

$$\zeta_{q,\nu}=-N_q\Lambda_\nu/(\omega_\nu+e_m-E), \tag{8}$$

where the normalization constant N_q is determined by the condition

$$\begin{aligned}1=\langle q|q\rangle&=\sum_{\nu,\nu'}\left[\delta_{\nu,\nu'}-\frac{\delta}{\delta E}W_{\nu\nu'}(E)\right]\Big|_{E=E_q}\zeta_{q,\nu}\zeta_{q,\nu'}\\&=N_q^2\{\sum_\nu\Lambda_\nu^2/(\omega_\nu+e_m-E_q)^2-[\sum_\nu\Lambda_\nu^2/(\omega_\nu+e_m-E_q)(E_q-\varepsilon_m-G)]^2\}\\&=N_q^2[\sum_\nu\Lambda_\nu^2/(\omega_\nu+e_m-E_q)^2-1],\end{aligned} \tag{9}$$

where use has been made of Eq. (7). In particular, the factor multiplying N_q^2 vanishes for $E_q=\varepsilon_m$, according to Eq. (7). There are thus only $\Omega-1$ states which have a finite renormalization. These are the physical eigenstates.

The calculation of both one- and two-body matrix elements for transfer operators within the NFT also reproduces the exact matrix elements for

transitions between physical states and vanishes identically for transitions between states such that at least one of them is unphysical.

The two unphysical roots appearing in this example have different origins: one is the unphysical linear combination of particle-phonon states (see the discussion after Eq. (3)); another corresponds to the three fermion states belonging to the complementary space. From Fig. 7 we see that this intermediate state has two-particle lines in the same m state and thus violates the Pauli principle. This spurious solution has appeared as a consequence of the Bloch-Horowitz formalism, since this formalism also yields the solutions corresponding to the complementary set.

In the previous example, the NFT Hamiltonian has been exactly diagonalized using the Bloch-Horowitz perturbation scheme. In particular, the matrix elements between the physical subset of states (proper states) have been obtained by summing to all orders of perturbation theory. In most situations, these exact summations cannot be carried out. The NFT will still be useful if a convenient perturbation scheme can be worked out.

A number of similar examples have appeared in the literature in order to verify the validity of the NFT.[6),18)~20)] Indeed, historically, the NFT rules were discovered through the treatment of these simplified but non-trivial cases.[6)]

§ 4. Perturbative application of the NFT

Let me here stress a point which has mislaid both friend and critics of the NFT: the Bloch-Horowitz perturbation technique (or, equivalently, the Wigner-Brillouin one if we deal with a single state in the physical subspace) is by no means indisolubly connected with the NFT. These perturbation schemes have been proved specially useful in problems which could be exactly solved through a summation of all orders of perturbation theory (as in the previous case). If we must stay within the lowest orders of perturbation theory, they have two important drawbacks:

i) Let us assume the Wigner-Brillouin case. The inclusion of the exact energy in the denominators includes some diagrams of higher order in the calculation of a particlar diagram (i.e., those which have at least an intermediate state equal to the initial state). In the Rayleigh-Schroedinger formalism, they appear with an oppositive sign to the other diagrams of the same (higher) order and in which all intermediate states are different from the ground state. Thus, we are selecting from the higher order contributions a subset which generally yields a wrong sign.

ii) Because of the non-linear problem implied by the presence of the exact energy in the denominator there are more roots than the dimension of the physical subspace in the Bloch-Horowitz case. In fact, all the energies

corresponding to the complementary space may appear. These are spurious states in NFT, as we have seen in the previous example. In actual calculations, it is desirable that at least this source of spurious states should be eliminated.

In the first place, we must discuss which is the appropriate expansion parameter associated with the NFT. This cannot be the strength of the interaction since the two-body vertices have already been summed to all orders of perturbation theory in order to obtain the RPA energies and vertices (see Figs. 2, 4 and 5).

We note that the boson energies and the particle-hole (or particle-particle) energies are of the same order of magnitude, which we take to be $O(1)$. In this unit, the two-body vertices are of $O(\Omega^{-1})$ (see Eq. (2) for the pairing case), where Ω is the total available degeneracy of the fermion space that can be used in the construction of the collective states. Similarly Eq. (3) suggests that the particle-phonon coupling vertices are of $O(\Omega^{-1/2})$. Let us assume that the phonons carry an angular momentum λ which is much smaller than Ω. In the limit $\lambda=0$, there is only one independent summation over all the fermion lines entering in a given fermion loop, since, for instance, any line entering in a particle-phonon vertex completely determines the exit one. Thus, each fermion loop yields a contribution of $O(\Omega)$ to the total diagram.

We choose Ω^{-1} as our expansion parameter. Therefore, a given diagram is of $O(\Omega^{(n_F-(1/2)n_A-n_v)})$, where n_F, n_A and n_v are the number of fermion loops, particle-phonon vertices and two-body vertices, respectively. For instance,

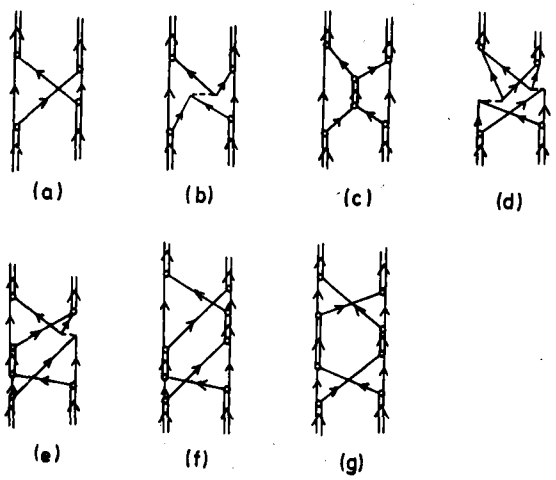

Fig. 9. The diagramatic NFT contributions to the pair addition phonon-phonon interaction. Graph (a) corresponds to $O(\Omega^{-1})$, while graphs (b)$\sim$(g), to the order $O(\Omega^{-2})$. The same diagrams are obtained for the case of removal phonons by inverting the sense of single- and double-arrowed lines.

the first diagram in Fig. 9 is of $O(\Omega^{-1})$, the second one of $O(\Omega^{-2})$, etc.

The convergence of the series in Ω^{-1} has been tested in the case of monopole neutron pairing phonons around Pb^{208} (see Fig. 9).[21] A pairing force has been exactly diagonalized on a basis of two and four particles (holes). The energy of the single-particle levels included in the calculation were taken from experiment. The pairing strengths were fixed so as to reproduce the experimental correlation energy of the one-phonon cases (1237 keV for the addition case and 640 keV for the removal case). The predicted two phonon addition state is 267 keV lower than the exact result, while the predicted two phonon removal state is 540 keV too low. This last (relatively large) quantity is of the same order of the phonon correlation energy, and is a consequence of the fact that the removal phonon is in the $(p_{1/2})^2$ configuration during 50% of the time. Problems associated with the Ω^{-1} convergence may thus be expected in this case.

Figure 9(a) displays the diagram of $O(\Omega^{-1})$, while diagrams (b)$\sim$(g) correspond to the $O(\Omega^{-2})$, according to the above classification. The NFT results, calculated using Rayleigh-Schroedinger perturbation theory, are displayed in Table III. In the removal case, already the Ω^{-1} contribution accounts for 90% of the exact value. The Ω^{-2} and Ω^{-3} contributions amount to 8% and 3% of the Ω^{-1} contribution. For the addition case the convergence is much faster, as expected.

Table III. Results of the diagonalization and of the NFT for the interaction energies associated with the two-pair addition (g.s. (^{212}Pb)) and two-pair removal (g.s. (^{204}Pb)) phonons (Ref. 21)).

Order	ΔW (keV)	
	I	II
$1/\Omega$	474	262
$1/\Omega^2$	42	4.3
$1/\Omega^3$	14	0.4
	530	266.7
Exact	540	267

If different configurations of proper states lie close to each other and if Ω is small, we cannot expect that first order perturbation theory could yield sufficiently good results. This was shown to be the case[22] for four particles moving in a $j\simeq 7/2$ shell and coupled by a force which is parametrized by the energies of the different λ-pairing phonons in the two-particle case. One also gets the exact results if one adds to infinite order all NFT diagrams.[20]

In such cases one may still use the diagrams of $O(\Omega^{-1})$ (Fig. 9(a)) in order to construct the matrix between the different two-phonon states (the improper states constitute again the complementary space). We avoid the Bloch-Horowitz energy denominators by using instead the difference between

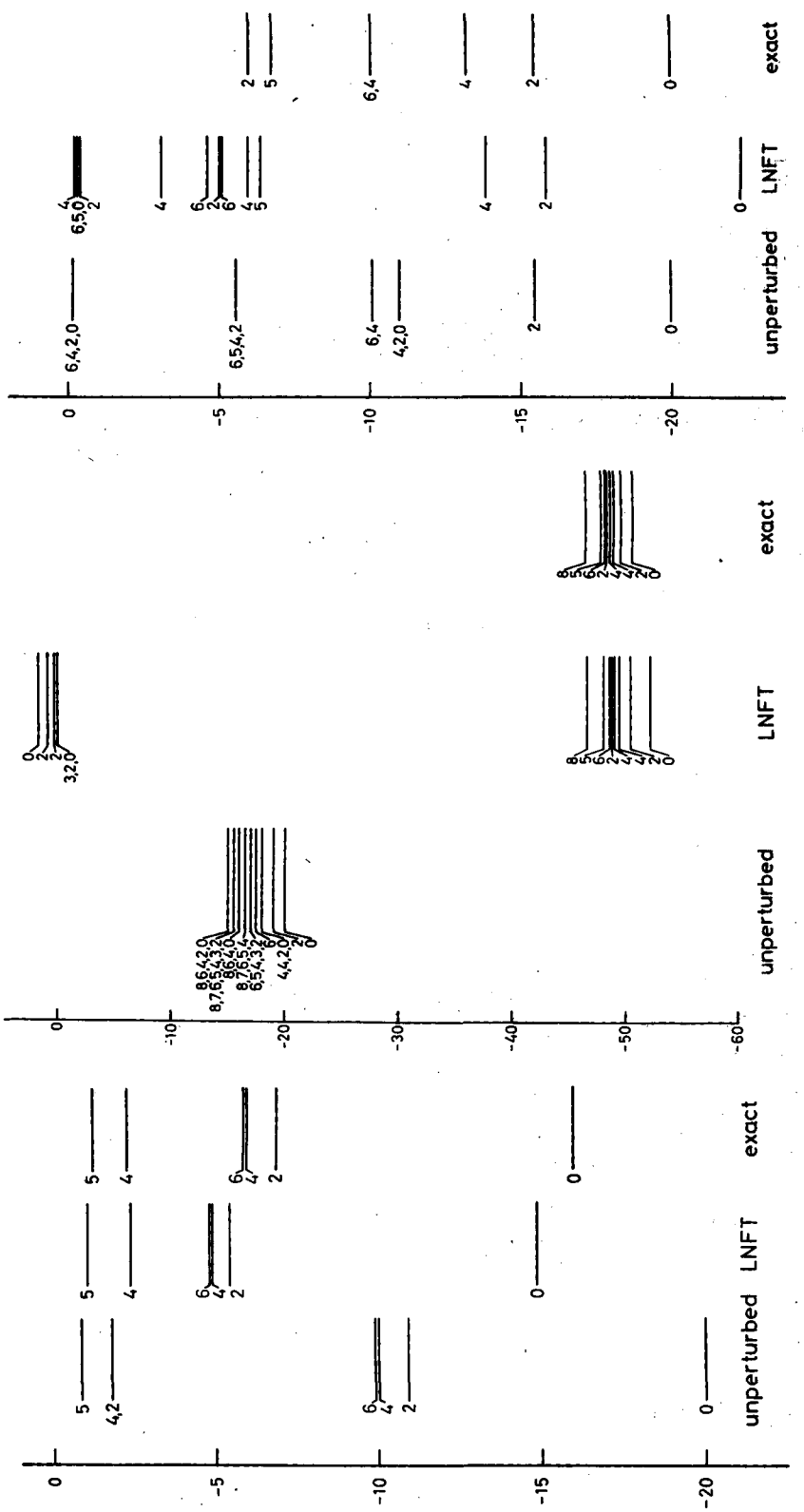

Fig. 10. The results of a diagonalization for four particles moving in a $j=7/2$ shell. The energies $W_0/W_2/W_4/W_6$ (where W_4 is the pairing phonon energy in the $(j)^4$ case) are (a) $-10/-1/-0.1/-0.1$; (b) $-10/-9/-8/-7$ and (c) $-10/-5.5/-0.1/-0.1$.

the energies of the initial and intermediate states. The validity of this prescription,[23] which yields non-hermitian matrices, is derived using the folding-diagrams formalism. Even for a small j-shell ($j=7/2$) one obtains good results (Figs. 10(a) and (b)). The diagonalization also yields a number of spurious states which have an imaginary norm. Furthermore, the energy of these spurious states is very close to zero. However, the results are not satifactory in Fig. 10(c). In this case the unperturbed energy of the two $\lambda=2$ phonon state (physical subspace) lies very close to the energy of the $\lambda=0$ phonon plus two-particle state (complementary space). More work is presently needed in order to understand such situations from the point of view of the NFT.

Another point which must be investigated is the convergence of the perturbation expansion in the neighbourhood of a phase transition.

One of the relatively few applications of the NFT has been carried out for the $3/2^+$ states in Bi^{209}.[24] These two states can be interpreted as a mixture of the octupole phonon coupled to a particle in the $h_{9/2}$ state and a proton $d_{5/2}$ hole created on the ground state of Po^{210}. The NFT calculation predicts a mixture of these two configurations which takes into account the underlying lack of orthogonality between both states. The calculation reproduces very well energies, inelastic scattering and transfer data (Table IV).

Use of the most important NFT diagrams has been made around closed shell nuclei also in Refs. 25) and 26) and in well deformed nuclei in Refs. 27) and 47). An application of the NFT to alpha-decay process is found in Ref. 28).

Table IV. The experimental and NFT theoretical values of the properties of the two lowest $3/2^+$ levels in Bi^{209} (Ref. 24)). The parameters entering in the NFT calculation are experimentally fixed through the single-particle and single-phonon spectrum. Application is made of the Bloch-Horowitz perturbation theory. Only Ω^{-1} terms are included in the calculation of each matrix element.

	Exp	NFT
E (MeV)	2.49	2.48
	2.95	3.07
$\frac{B(E3;\,2.49\,\text{MeV})}{B(E3;\,2.95\,\text{MeV})}$	3.8+0.8	2.5
$\frac{\sigma(t,\alpha;\,2.49\,\text{MeV})}{\sigma(t,\alpha;\,2.95\,\text{MeV})}$	0.8+0.3	0.8

§ 5. A number conserving derivation of the BCS equations

In this section we study again the problem of particles moving in a given set of single-particle levels and being coupled by a monopole pairing force. In zero order, the ground state of a system with 2Π particles is represented as a superposition of Π independent monopole pairing bosons while it has an

additional particle line in the odd system with $2\Pi+1$ particles. This description can be corrected using NFT diagrams, which may be ordered according to the power of Ω^{-1} (see § 4). However, in the present case it is more reasonable to use an expansion in two parameters, Ω^{-1} and Π/Ω. For an arbitrary matrix element,

$$F(\Omega^{-1}, \Pi/\Omega) = \sum_{a,b} \Omega^{-b} (\Pi/\Omega)^a. \tag{1}$$

We will consider the lowest value of b and we will sum all the series in a. Thus, we assume $\Omega \gg 1$ and Π/Ω finite.

The Hamiltonian, boson frequencies and particle-phonon interaction vertices are given in Eqs. (1)$\sim$(3) of § 3.

We define the principal series approximation (PSA) as being given by those diagrams with the smallest difference between the number of loop p and the number of internal connections s. These connections may represent either an (instantaneous) interaction given by the particle-particle vertex or a (delayed) interaction involving the emission and absorption of a phonon. For instance, there is a subset of diagrams in which the difference $p-s$ vanishes for the ground state of an odd system (Fig. 11). The PSA includes those diagrams which minimize the exponent of Ω^{-1}, if the contributions of the

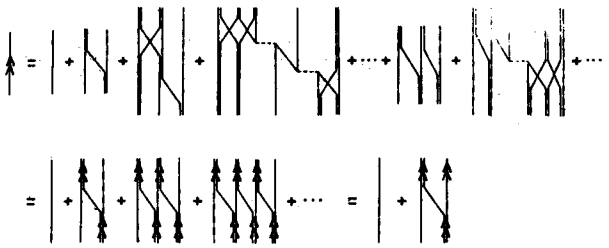

Diagrams and Dyson equation defining the quasiparticles within the PSA.

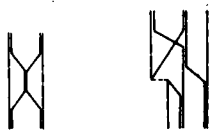

Examples of diagrams not included in the PSA.

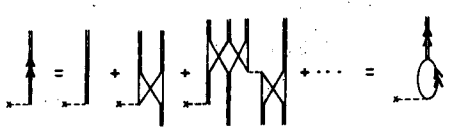

The self-consistency condition for the pairing momentum within PSA.

Fig. 11. The graphical perturbation expansion included the BCS super-fluid solution (Ref. 29)).

vertices of the external phonons are not counted. This is so because we keep Π/Ω finite, and for each factor $\Omega^{-1/2}$ thus appearing there is a factor of $\Pi^{1/2}$ due to the presence of Π external bosons. A PSA diagram is characterized by the fact that it becomes separated into two disconnected diagrams by severing it through a connection. All diagrams in the first and the last row of Fig. 11 belong to the PSA, while those in the third row do not.

The set of PSA diagrams corresponding to the odd system defines quasiparticle excitations, which are represented by a single line with a double arrow. The initial and final particle lines follow a zig-zag path (first row in Fig. 11). In each of the vertices of this path, two particles are created or annihilated. Each vertex is connected with a part of the diagram which represents a PSA contribution to the two-particle creation or annihilation amplitude $\langle \Pi+1|c_m^\dagger c_{\bar{m}}^\dagger|\Pi\rangle$ (last row in Fig. 11). This amplitude is also given by the residues of the two-particle Green's function, if the pairing phonons are consistently calculated within the PSA. The renormalized pairing bosons are represented by the parallel lines crossed by two arrows. Since these bosons may be expressed in terms of the propagation of particles and quasiparticles, the odd system becomes coupled with the even system. In the following, we derive the corresponding equations.

The diagrams in the first row of Fig. 11 are ordered according to the number of vertices appearing in the initial and final particle lines. Consequently with the previous discussion, each vertex creates or annihilates a renormalized phonon as shown in the first member of the equality in the second row. These processes give rise to a Dyson-type equation for the quasiparticles. In this equations, we must also take into account the (implicit) propagation of unconnected bosons,

$$\begin{aligned} G(m;t'-t)F_\Pi(T'-T) &= G_0(m;t'-t)F_\Pi(T'-T) + \Delta_m^2 F_{\Pi-1}(T'-T) \\ &\times \int d\tau d\tau' G_0(m;\tau'-t)G_B(\tau-T)G_0(\bar{m};\tau'-\tau) \\ &\times G_B(T'-\tau')G(m;t'-\tau), \end{aligned} \tag{2}$$

where the single-particle and single-boson propagators are (Eqs. (3) and (6) in § 2)

$$\begin{aligned} G_0(m;t) &= e^{-i\varepsilon_m t}\theta(t)\ , \\ G_B(t) &= e^{-i2\sigma t}\theta(t)\ . \end{aligned} \tag{3}$$

Here, 2σ denotes the frequency of the dressed phonons. The factor $F_\Pi(T'-T)$ corresponds to the free propagation of Π phonons between the times $T<t$ and $T'>t'$. A dressed boson gives rise to a pair of time-reversed fermion lines $(m, \bar{m})$ in a vertex of renormalized strength Δ_m. This vertex includes a factor $\Pi^{1/2}$, arising from the fact that each vertex on the left-hand member of the second row in Fig. 11 yields a factor

$$\Pi!/(\Pi-v)!\approx\Pi^v, \qquad \text{if} \quad \Pi\gg v, \tag{4}$$

where v is the number of connected initial or final external bosons.

The quasiparticle propagator is written in the Lehman representation,

$$G(m;t)=U_m^2\exp[-iE_m^{(a)}t]\theta(t)-V_m^2\exp[-iE_m^{(r)}t]\theta(-t), \tag{5}$$

where

$$U_m=\langle a, m|c_m^\dagger|0\rangle, \quad V_m=\langle r, m|c_m|0\rangle, \tag{6}$$

are the amplitudes of the advanced and retarded parts, respectively, while $E_m^{(a)}$ and $E_m^{(r)}$ denote the corresponding energies.

After Fourier transformation, Eq. (2) becomes equivalent to

$$\begin{aligned}U_m^2/(k-E_m^{(a)})+V_m^2/(k-E_m^{(r)})&=1/(k-e_m)+[U_m^2/(k-E_m^{(a)})\\&\quad+V_m^2/(k-E_m^{(r)})]\Delta_m^2/(k-e_m)(k+e_m-2\sigma).\end{aligned} \tag{7}$$

Analiticity at the poles $E_m^{(s)}$ requires $(s=a, r)$

$$\begin{aligned}&\Delta_m^2/(E_m^{(s)}+e_m-2\sigma)(E_m^{(s)}-e_m)=1,\\&E_m^{(a)}=\sigma+E_m, \quad E_m^{(r)}=\sigma-E_m, \quad E_m=[(e_m-\sigma)^2+\Delta_m^2]^{1/2}.\end{aligned} \tag{8}$$

Similarly, the poles at e_m and $2\sigma-e_m$ yield the equations

$$\begin{aligned}&U_m^2/(E_m-e_m+\sigma)-V_m^2/(E_m+e_m-\sigma)=2(e_m-\sigma)/\Delta_m^2,\\&U_m^2/(E_m+e_m-\sigma)-V_m^2/(E_m-e_m+\sigma)=0,\end{aligned} \tag{9}$$

from which the square of the amplitudes U_m and V_m is obtained, namely

$$\begin{aligned}U_m^2&=[1+(e_m-\sigma)/E_m]^{1/2},\\V_m^2&=[1-(e_m-\sigma)/E_m]^{1/2}.\end{aligned} \tag{10}$$

The graphical equation*) for the PSA phonons is displayed in the last row of Fig. 11.

$$\begin{aligned}\langle\Pi+1|c_m^\dagger c_{\bar m}^\dagger|\Pi\rangle&=\Delta_m U_m^2/(2\sigma-e_m-E_m^{(a)})\\&=-\Delta_m U_m^2/(E_m+e_m-\sigma)=-\Delta_m/2E_m,\end{aligned} \tag{11}$$

where use of Eq. (10) has been made. The vertex Δ_m is given by an equation similar to (3·3)

$$\Delta_m=\sum_n{}'\langle m, \bar m|H'|n, \bar n\rangle\langle\Pi+1|c_n^\dagger c_{\bar n}^\dagger|\Pi\rangle$$

---

*) Note that the intermediate state now includes the propagation of a particle and a quasiparticle line. The propagation of two-quasiparticles would overcount the PSA processes, as may be verified through successive iterations.

$$= -V\langle \Pi+1|\sum_n{}' c_n^\dagger c_{\bar{n}}^\dagger|\Pi\rangle\,. \tag{12}$$

Summation over n yields the familiar gap equation, which for a pairing force (Eq. (1) in § 3) with constant matrix elements reads

$$2/V=\sum_m{}' 1/E_m\,. \tag{13}$$

In the normalization condition, we must exclude from the interaction vertices a factor $\Pi^{1/2}$ which was included due to the presence of Π external pairing bosons

$$\begin{aligned} 1&=\sum[\langle \Pi+1|c_m^\dagger c_{\bar{m}}^\dagger|\Pi\rangle]^2=\sum[\Delta_m U_m/(E_m-e_m-\sigma)]^2/\Pi \\ &=\sum[1-(e_m-\sigma)/E_m]/2\Pi\,, \end{aligned} \tag{14}$$

which is the usual number equation, namely

$$\Pi=\sum V_m{}^2\,. \tag{15}$$

The BCS equations are thus derived[29] starting from the NFT basis of independent particles and TDA pairing phonons, making in its derivation two approximations:

i) The restriction to a certain subset of diagrams, namely, the ones belonging to the PSA.

ii) The replacement in Eq. (4).

In the limit of large Ω, (but finite Π/Ω) the PSA diagrams are the only ones contributing to an (exact) description of the system. In this limit the excitations of the system are defined by the gap and number BCS equations. We have learned, in particular, which particle diagrams are implicitly taken into account in the superfluid solution. In this limit it is simpler to use the BCS formalism rather than the PSA. However, there are problems associated with perturbation theory in deformed basis which are treated in the following section.

The extension of this derivation to the general Nilsson-Bogolubov transformation has been performed for an arbitrary force.[30]

§ 6. Rotations and the perturbative treatment of fermion systems in deformed basis

Attempts to extend the NFT formalism to the case of rotations were started as soon as the vibrational case was understood. The success of these attempts was made plausible by the analogy between the product space of intrinsic (fermion) and collective degrees of freedom characteristic both of the unified model and of the NFT spaces, by the similarity between the Coriolis coupling and the particle-phonon interaction, etc. However, all these

attempts led to failures. This may be explained as follows:

The total Hamiltonian $H(a_m^\dagger, a_m)$ of a system of fermions may be written in two parts $H_0+H_{\rm res}$. We consider the case in which the basic set of states (eigenfunctions of H_0) is deformed, i.e., $[H, L_\nu]=0$ and $[H_0, L_\nu]\neq 0$, where L_ν can be components of the angular momentum, the number of particles, etc. Since the inclusion of $H_{\rm res}$ restores the original symmetry of the problem, a perturbative treatment of $H_{\rm res}$ would imply a perturbative transformation from the deformed to the spherical basis. This cannot exist, since the opposite transformation (from the normal to the deformed basis) is known to be non-perturbative. The origin of these difficulties can be traced back to the absence of restoring force in the angular direction for a freely rotating system, giving rise to infrared catastrophes.

In Ref. 31) a procedure to overcome these difficulties is derived.

As in the previous formulation of the NFT, the present chapter may be divided into two sections. In the first subsection 6. 1 a formal derivation is made of a Hamiltonian in which both the rotational and the single-particle degrees of freedom explicitly appear. In the second section 6. 2, the discussion is centered on how to treat this Hamiltonian.

6. 1. The philosophy in this section is similar to the one in §§ 2 and 5: the equivalence between a pure fermion Hamiltonian and a Hamiltonian including both the fermion and the collective (rotational) degrees of freedom is proven by the fact that they yield the same (vacuum) transition amplitude (as given in this case by the path-integral formalism).

Let us consider a system of interacting fermions described by a set of creation and destruction operators $b_m^\dagger, b_m$, where the index m refers to all the quantum numbers that label the independent particle states. The Hamiltonian of the system is assumed to commute with the components of the angular momentum $L_\nu(b_m^\dagger, b_m)$ so that the Lagrangian $L=i\sum_m b_m^\dagger \dot{b}_m - H$ is invariant under a (time-independent) rotational transformation $R(\phi)$ which is parametrized by the three Eular angles ϕ_ν. Let us denote

$$a_m^\dagger = a_m^\dagger(\phi) = R(\phi)\, b_m^\dagger . \tag{1}$$

We use the path-integral formulation of Ref. 32). Thus, we consider the ground to ground transition amplitude

$$Z=\prod_m \int D[b_m^\dagger] D[b_m] \exp\left(i\int L dt\right) \tag{2}$$

which may also be written in terms of a path integral in which the rotational degrees of freedom are separated. Two main steps are necessary in order to carry out this transformation (c.f. Ref. 33), Appendix A).

(i) Ones uses two expressions for unity

$$1=\prod_v \int D[I_v]\delta(I_v-L_v(a_m^\dagger, a_m)), \tag{3}$$

$$1=\prod_v \int D[\phi_v]\delta(\theta_v(a_m^\dagger, a_m)-\bar{\theta}_v)\det\left(\frac{\partial\theta_u(a_m^\dagger, a_m)}{\partial\phi_w}\right)$$

$$=\prod_v \int D[\phi_v]\delta(\theta_v-\bar{\theta}_v)\det(U_{uw}(\phi))\det([L_u, \theta_w]_{PB}), \tag{4}$$

where $\bar{\theta}_v$ is a constant and we have (consecutively) used the definition of Poisson brackets, the linear transformation U between the cartesian components of the angular momentum I_v and the momenta Π_v which are conjugate to the Euler angles and the constraint implied by Eq. (3).

(ii) One expresses the kinetic fermion term $i\sum_m b_m^\dagger \dot{b}_m$ in terms of the rotated fields $a_m^\dagger$, $\dot{a}_m$ and the collective variables I_v, $\dot{\phi}_v$.

$$\sum_m b_m^\dagger \dot{b}_m = \sum_m a_m^\dagger \dot{a}_m - i\sum_v \Pi_v \dot{\phi}_v . \tag{5}$$

Therefore one multiplies (2) by (3) and (4) and substitutes (5), thus yielding

$$Z=\prod_{m,v}\int D[a_m^\dagger]D[a_m]D[I_v]D[\phi_v]$$
$$\times\delta(I_v-L_v)\cdot\delta(\theta_v-\bar{\theta}_v)\cdot\det([L_u, \theta_w]_{PB})\cdot\det(U_{uw}(\phi_v))$$
$$\times\exp\left[-\int\left(\sum_m a_m^\dagger\dot{a}_m - i\sum_v \Pi_v\dot{\phi}_v + iH\right)dt\right]. \tag{6}$$

The determinant of the linear transformation U has the value $\sin\beta$.[34] Thus,

$$\prod_v d\phi_v \det(U_{uw}(\phi_v)) = \sin\beta\, d\alpha d\beta d\gamma = d\Omega \tag{7}$$

is the usual expression for the differential involving Euler angles.

The angular momentum constraint is straightforwardly exponentiated. Apart from a normalization constant, one obtains

$$Z=\lim_{D\to 0}\prod_{m,v}\int D[a_m^\dagger]D[a_m]D[I_v]D[\Omega]$$
$$\times\delta(\theta_v-\bar{\theta}_v)\cdot\det([L_u, \theta_w]_{PB})$$
$$\times\exp\left[-i\int\left(-i\sum_m a_m^\dagger\dot{a}_m - \sum_v \Pi_v\dot{\phi}_v + H + \frac{1}{2D}\sum_v (I_v-L_v)^2\right)\right]. \tag{8}$$

The $\theta_v(a_m^\dagger, a_m)$ are functions of the fermion fields. They are quite arbitrary but for the condition that the determinant of the Poisson bracket $[\ ]_{PB}$ must not vanish. It is convenient to relate them to the angular variables conjugate to the L_v. Therefore, the gauge condition $\delta(\theta_v-\bar{\theta}_v)$ fixes

the position of the intrinsic frame of reference relative to the rotating body and eliminates the rotations of the total system as degrees of freedom associated with the fermion fields. Since the physical results must be independent of the angular eigenvalues $\bar{\theta}_\nu$, one may construct a wave packet around $\bar{\theta}_\nu=0$. This yields

$$Z=\lim_{D\to 0}\prod_{m,\nu}\int D[a_m^\dagger]D[a_m]D[I_\nu]D[\Omega]\det([L_w,\theta_u]_{PB})$$
$$\times\exp\Big[-i\int\Big(-i\sum_m a_m^\dagger\dot{a}_m-\sum_\nu \Pi_\nu\dot{\phi}_\nu+H+\frac{1}{2D}\sum_\nu(I_\nu-L_\nu)^2$$
$$+\frac{1}{2A}\sum_\nu\theta_\nu^2\Big)dt\Big]. \tag{9}$$

The final physical results must be independent of the width A.

In principle, it is possible to choose the θ_ν such that the determinant of the Poisson brackets equals one (to the order Q^{-1} to which the calculation is carried). In this case, the determinant in (9) is trivially taken into account: Although this procedure is used in Refs. 35) and 8), it is not the only possible one, since the determinant may also be exponentiated:

$$Z=\lim_{D\to 0}\prod_{m,\nu}\int D[a_m^\dagger]D[a_m]D[I_\nu]D[\Omega]$$
$$\times\exp\Big[-i\int\Big(-i\sum_m a_m^\dagger\dot{a}_m-\sum_\nu \Pi_\nu\dot{\phi}_\nu+H+\frac{1}{2D}\sum_\nu(I_\nu-L_\nu)^2$$
$$+\frac{1}{2A}\sum_\nu\theta_\nu^2+V\ln(\det([L_w,\theta_u]_{PB}))\Big)dt\Big]. \tag{10}$$

The logarithm in the exponent can be expanded if the θ_ν are chosen such that the leading order term in the determinant is one. This is a lesser requirement than the earlier choice of θ_ν.

Therefore we have achieved our purpose, since the same vacuum transition amplitude can be obtained a) from a Hamiltonian involving only fermion degrees of freedom $(b_m^\dagger, b_m)$; and b) from a treatment in which the collective degrees of freedom (I_ν, ϕ_ν) are explicitly separated from the fermion variables $(a_m^\dagger, a_m)$ and in which the constraints are taken into account as additional terms in the effective Hamiltonian.

6. 2. Up to a constant, the Hamiltonian H is equivalent to H'

$$H'=\lim_{D\to 0}\Big[H+\frac{1}{2D}\sum_\nu(I_\nu-L_\nu)^2+\frac{1}{2A}\sum_\nu\theta_\nu^2$$
$$+V\sum_n(1-\det(i[L_\nu,\theta_u]))^n/n\Big]. \tag{11}$$

The following points may be stressed:

1) The Hamiltonian H' acts on wave functions belonging to the product space used in the unified model

$$\Psi_{I,M,K,n}(\phi_v, a_m^\dagger, a_m) = D^I_{M,K}(\phi_v) f_{I,K,n}(a_m^\dagger, a_m). \tag{12}$$

One has in mind an independent-particle basis for the intrinsic states $f_{I,K,n}$.

2) The quadrupole operators in configuration space are written:

$$Q_v = -2\cdot 3^{1/2} \sum_i (x^2_{v+1} - x^2_{v+2})_i, \quad (v = x, y, z = 1, 2, 3)$$

$$S_v = -2\cdot 3^{1/2} \sum_i (x_{v+1} x_{v+2})_i. \tag{13}$$

The usual choice of intrinsic frame implies that the expectation values $\bar{S}_v$ vanish. On the contrary, the expectation values $\bar{Q}_v$ are assumed to be large, at least in the determinantal ground state. Therefore, the operators Q_v are split into a large constant term $\bar{Q}_v$ and a term Q_v' that has matrix elements of the order of single-particle values and therefore are of $O(1)$ (much smaller than the $\bar{Q}_v$'s). The operators S_v have particle-hole matrix elements and can be considered to be of order $\bar{Q}_v^{1/2}$, since the expectation values of S_v^2 are of order $\bar{Q}_v$. The same is assumed for the angular momentum components L_v. Therefore, the expansion parameter Q^{-1} is taken to be the inverse of any of the three static moments Q_v.

Using these general estimates in connection with Eq. (13), the angular function θ_v can be approximated by

$$\theta_v = S_v/\bar{Q}_v. \tag{14}$$

Due to the absence of a restoring force in the angular direction, there is no contribution from H to the frequency of the angular oscillation (Goldstone boson). On the contrary, the appearance in the constrained Hamiltonian H' of the three harmonic oscillators

$$h_v = (1/2D) L_v^2 + (1/2A)\theta_v^2 \tag{15}$$

yields oscillations along the three axis of rotation with the (common) frequency

$$w = 1/(AD)^{1/2}. \tag{16}$$

Consequently, the spurious states are eliminated from the spectrum as D vanishes. However, they must always be used as intermediate states. The limit $D\to 0$ can only be taken in the final physical results. Moreover, in this limit the results must be independent of the parameter A.

3) Using the expression (14) for the angular functions, the determinant appearing in the constrained Hamiltonian is

$$1 + \sum_v Q_v'/\bar{Q}_v + \sum_v S_v^2/\bar{Q}_{v+1}\bar{Q}_{v+2} + O(Q^{-3/2}). \tag{17}$$

Unlike the constant A, V is not an arbitrary parameter. Its value has been determined from the conditions that the terms (17) yield the same results as the terms appearing in θ_v^2 if the determinant is set to be $1+O\ (Q^{-3/2})$. In all cases that we have studied so far

$$V=-\bar{\theta}_v^2/A\,. \tag{18}$$

4) Treatment of the constrained Hamiltonian. The original Hamiltonian H is written in the rotating frame of reference, thus defining a single-particle (deformed) basis and a residual Hamiltonian acting among the Nilsson particles. Neither the independent-particle terms, nor the residual Hamiltonian separately have the spherical symmetry of the total H. This step is common to most treatments of deformed systems. Next, one writes the other contributions to the effective Hamiltonian in the representation thus defined.

The Coriolis term $\sum_v I_v L_v/D$ is of $O(Q^{1/2})$ and thus not sufficiently small from the point of view of the Q-dependence. It is eliminated (as well as the rotation term $(1/2D)\sum_v I_v^2$) by means of the transformation

$$H_{\text{eff}}=e^{iT}H'e^{-iT}\,,$$
$$T=-\sum_v I_v\theta_v\,. \tag{19}$$

Only the commutation of H and T contributes in H_{eff} to the $O(1)$ of the rotational energy, and the corresponding terms yields the Thouless-Valatin moment of inertia.[36),37)] However, the aim of the present formalism is to go beyond this order.

The resultant Hamiltonian H_{eff} includes arbitrarily large residual interactions ($D\to 0$). These may be conveniently treated within the NFT formalism, which also allows to cast the results into a power series in Q^{-1}.

5) Application to the Elliott model:

The $SU(3)$ Elliott model[38)] consists of particles moving in a harmonic oscillator shell and coupled through quadrupole forces. This model yields an exact rotational spectrum $I(I+1)$, the excitation energies of the different band-heads and quadrupole matrix elements within a rotational band. These physical magnitudes are exactly reproduced to the order of the expansion in Q^{-1} to which our calculation is made. This is at least an order of magnitude higher than the one corresponding to the semiclassical approximation (cranking model).[33)]

As an example, we calculate the matrix elements of the quadrupole operator in the ground-state band. After the transformation (19), the $K=0$ component of the quadrupole operator reads*)

*) Terms of $O(Q^{-1})$ which are not dependent on angular momentum operators are omitted.

$$Q_M^{(\mathrm{eff})}|_{K=0}=e^{iT}Q_M^{(\mathrm{lab})}|_{K=0}$$
$$=D_{M0}^2(\phi)\left[\bar{Q}_\beta+Q_\beta'+\frac{3^{1/2}}{2}\left(\frac{S_x^2}{\bar{Q}_x}+\frac{S_y^2}{\bar{Q}_y}\right)+\frac{3^{3/2}}{2}\left(\frac{I_y^2}{\bar{Q}_y}-\frac{I_x^2}{\bar{Q}_x}\right)+O(Q^{-2})\right], \tag{20}$$

where $Q_\beta=(Q_x-Q_y)/(2\sqrt{3})$. The expectation value of (20) in the intrinsic vacuum states reads

$$\langle Q_M^{(\mathrm{eff})}\rangle|_{K=0}=D_{M0}^2(\phi)\left[\bar{Q}_\beta+\frac{3\bar{Q}_\beta}{2wD}+\frac{3^{3/2}}{2}\left(\frac{I_y^2}{\bar{Q}_y}-\frac{I_x^2}{\bar{Q}_x}\right)+O(Q^{-2})\right], \tag{21}$$

which clearly diverges as $D\to 0$. However, we may only expect that the *total* value of the matrix element converges. Thus, we must add to (21) the value of the diagram in Fig. 12, namely,

$$\langle Q_M^{(\mathrm{eff})}\rangle|_{K=0}=D_{M0}^2\left(-\frac{3\bar{Q}_\beta}{2wD}+3\right). \tag{22}$$

The sum of (21) and (22) is i) finite and independent of A and ii) contains a correction $(=3)$ of $O(Q^{(0)})$ and a centrifugal stretching term of $O(Q^{-1})$:

$$\langle Q_M^{(\mathrm{eff})}\rangle|_{K=0}=D_{M0}^2\left[\bar{Q}_\beta+3+\frac{3^{3/2}}{2}\left(\frac{I_y^2}{\bar{Q}_y}-\frac{I_x^2}{\bar{Q}_x}\right)\right]. \tag{23}$$

We similarly obtain, for $Q_\tau=-(Q_x+Q_y)/2$,

$$\langle Q_M^{(\mathrm{eff})}\rangle|_{K=2}=\frac{1}{\sqrt{2}}(D_{M2}^2+D_{M-2}^2)\left[\bar{Q}_\tau+\sqrt{3}+\frac{3}{2}\left(\frac{I_z^2}{\bar{Q}_z}-\frac{I_x^2}{\bar{Q}_x}-\frac{I_y^2}{\bar{Q}_y}\right)\right]. \tag{24}$$

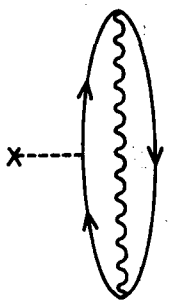

Fig. 12. Diagramatic contribution to the quadrupole operator in the ground state band. The cross denotes a vertex given by operator Q_β'.

The Elliott model does not provide us with a direct check of (23) and (24). However, these matrix elements may be verified through the replacement of both equations in the quadrupole Hamiltonian, yielding

$$E=-\frac{\chi}{2}(\bar{Q}_\beta^2+\bar{Q}_\tau^2+2\sqrt{3}\bar{Q}_x)+\frac{3\chi}{2}I(I+1) \tag{25}$$

which is the exact expression for the energy.[38]

Rotations in two dimensions have been treated in Refs. 31), 35) and 8). The relation between our approach and the Marshalek-Weneser expansion for the rotational case[39),40)] as well as illustrative clarifications on the present method, have recently been given by Marshalek,[41)] for the two-dimensional case. The two-dimensional pairing rotor has also been treated by Matsuyanagi et al.[42)] using modified fermion commutation relations, which include the effects of the constraints. For the three-dimensional case see also Refs. 43), 44) and 45).

§ 7. Conclusions

A perturbative scheme has been achieved which treates both vibrational and fermion degrees of freedom (or rotational, vibrational and fermion degrees of freedom) on an equal footing. The formalism yields exact results, to the order in which the perturbation is carried out. However, it cannot get across a phase transition.

Acknowledgements

Discussions both in Buenos Aires and Copenhagen have been essential in order to construct the NFT. The formalism corresponding to the rotational case was developed at Orsay.

Although almost all the work presented in these lectures has already been published, so far there has been no available reasonable presentation of the NFT. I regret some misunderstandings that this fact has produced. Because of this reason, I am specially thankful to Professor M. Yamamura and the Advisory Committee of the 5th Kyoto Summer Institute for this opportunity to lecture at the KSI and to Professor T. Marumori for the invitation to visit Japan.

A fellowship from the Japan Society for the Promotion of Science is deeply appreciated.

References

1) L. Landau, J. of Phys. (USSR) **5** (1941), 71.
2) A. Bohr and B. R. Mottelson, *Nuclear Structure*, vol. II (W. A. Benjamin, Inc., Reading, Mass.).
3) B. R. Mottelson, *Elementary Modes of Excitation in Nuclei*, ed. A. Bohr and R. A. Broglia (Academic Press, New York, 1977).
4) P. Nozieres, *Theory of Interacting Fermi Systems* (W. A. Benjamin, Inc., New York).
5) A. B. Migdal, *Theory of Finite Fermi Systems and Applications to Atomic Nuclei* (Interscience, New York).
6) D. R. Bes, G. G. Dussel, R. A. Broglia, R. Liotta and B. R. Mottelson, Phys. Letters **52B** (1974), 253.
7) D. R. Bes, G. G. Dussel, R. P. J. Perazzo and H. M. Sofia, Nucl. Phys. **A307** (1978), 402.
8) D. R. Bes, G. G. Dussel and R. P. J. Perazzo, Nucl. Phys. **A340** (1980), 157.

9) D. R. Bes, R. A. Broglia, G. G. Dussel, R. J. Liotta and R. P. J. Perazzo, Nucl. Phys. **A260** (1976), 77.
10) D. R. Bes and R. A. Broglia, *Proceedings of the Topical Conference on Problems of Vibrational Nuclei, Zagreb, September, 1974* (North-Holland Publishing Co., Amsterdam, 1975), p. 1.
11) H. Reinhardt, Nucl. Phys. **A251** (1975), 317.
12) H. Reinhardt, Nucl. Phys. **A298** (1978), 77.
13) S. Iwasaki, P. Ring and P. Shuck, Nucl. Phys. **A331** (1979), 81.
14) P. Schuck, S. Iwasaki and P. Ring, *Proceedings of the Nuclear Physics Workshop, ICTP, Trieste, 1981*, ed. C. H. Dasso, R. A. Broglia and A. Winther (North-Holland, Amsterdam, 1982).
15) B. R. Mottelson, J. Phys. Soc. Japan Suppl. **24** (1968), 87.
16) R. A. Broglia, B. R. Mottelson, D. R. Bes, R. Liotta and H. M. Sofia, Phys. Letters **64B** (1976), 29.
17) D. R. Bes and R. A. Broglia, *Elementary Modes of Excitation in Nuclei*, ed. A. Bohr and R. A. Broglia (Academic Press, New York, 1977), p. 55.
18) D. R. Bes, R. A. Broglia, G. G. Dussel and R. J. Liotta, Phys. Letters **56B** (1975), 104.
19) D. R. Bes, R. A. Broglia, G. G. Dussel, R. J. Liotta and H. M. Sofia, Nucl. Phys. **A260** (1976), 1, 27.
20) C. L. Wu, Nucl. Phys. **A349** (1980), 114.
21) P. F. Bortignon, R. A. Broglia and D. R. Bes, Phys. Letters **76B** (1978), 153.
22) C. L. Wu and D. H. Feng, Phys. Rev. **C24** (1981), 727.
23) N. N. Scoccola and D. R. Bes, to be published.
24) P. F. Bortignon, R. A. Broglia, D. R. Bes and R. J. Liotta, Phys. Reports **30C** (1977), 309.
25) I. Hamamoto, Phys. Reports **10C** (1974), 63.
26) P. Kleinheinz, J. Styczen, M. Piiparinen, J. Blomqvist and M. Kortelaht, Phys. Rev. Letters **48** (1982), 1457.
27) I. Hamamoto, Prog. Theor. Phys. Suppl. Nos. 74 & 75 (1983), 157.
28) F. A. Janouch and R. Liotta, Nucl. Phys. **A334** (1980), 427.
29) G. G. Dussel and D. R. Bes, Nucl. Phys. **A323** (1979), 392.
30) J. Dukelsky, Thesis, Instituto Balseiro, University of Cuyo, Argentina, 1982.
31) V. Alessandrini, D. R. Bes and V. Machet, Nucl. Phys. **B142** (1978), 489.
32) J. L. Gervais, A. Jevicki and B. Sakita, Phys. Reports **23C** (1976), 281.
33) D. R. Bes, O. Civitarese and H. M. Sofia, Nucl. Phys. **A370** (1981), 99.
34) J. M. Eisenberg and W. Greiner, *Nuclear Theory*, vol. 3 (North-Holland, Amsterdam, 1976).
35) V. Alessandrini, D. R. Bes and V. Machet, Phys. Letters **80B** (1978), 9.
36) F. M. H. Villars, Nucl. Phys. **74** (1965), 353.
37) F. M. H. Villars and G. Cooper, Ann. of Phys. **56** (1970), 224.
38) J. P. Elliott, *Selected Topics in Nuclear Theory*, ed. F. Janouch (IAEA, Vienna, 1963).
39) E. R. Marshalek and J. Weneser, Ann. of Phys. **53** (1969), 569.
40) E. R. Marshalek and J. Weneser, Phys. Rev. **C2** (1970), 1682.
41) E. R. Marshalek, Preprint and *Proceedings of the INS Symposium on Dynamics of Nuclear Collective Motion, Mt. Fuji, 1982* (to be published).
42) K. Matsuyanagi, *Proceedings of the Nuclear Physics Workshop, ICTP, Trieste, 1981*, ed. C. H. Dasso, R. A. Broglia and A. Winther (North-Holland, Amsterdam, 1982), p. 29.
43) V. G. Zelevinsky, Nucl. Phys. **A344** (1980), 109.
44) H. Reinhardt, Nucl. Phys. **A381** (1982), 217.
45) E. R. Marshalek, Nucl. Phys. **A381** (1982), 240.
46) D. G. Kovar, N. Stein and C. K. Bockelman, Nucl. Phys. **A231** (1974), 266.
47) T. S. Dumitrescu and I. Hamamoto, Nucl. Phys. **A383** (1982), 205.